The cellular response towards lanthanum is substrate specific and reveals a novel route for glycerol metabolism in *Pseudomonas putida* KT2440

Matthias Wehrmann[a], Maxime Toussaint[b, c], Jens Pfannstiel[d], Patrick Billard[b, c#], Janosch Klebensberger[a#]

[a]*University of Stuttgart, Institute of Biochemistry and Technical Biochemistry, Department of Technical Biochemistry, Stuttgart, Germany*

[b]*Université de Lorraine, LIEC UMR7360, Faculté des Sciences et Technologies, Vandoeuvre-lès-Nancy, France*

[c]*CNRS, LIEC UMR7360, Faculté des Sciences et Technologies, Vandoeuvre-lès-Nancy, France*

[d]*Core Facility Hohenheim, Mass Spectrometry Module, University of Hohenheim, August von Hartmann-Str. 3, 70599 Stuttgart, Germany*

Running title: Conditional responses of *Pseudomonas putida* towards rare earth elements

#Address correspondence to Janosch Klebensberger (janosch.klebensberger@itb.uni-stuttgart.de) and Patrick Billard (patrick.billard@univ-lorraine.fr)

Keywords: Lanthanides, rare earth elements, proteome, glycerol metabolism, *Pseudomonas putida*, PQQ, PedE, PedH, GarK, dehydrogenases

Abstract

Ever since the discovery of the first rare earth element (REE)-dependent enzyme, the physiological role of lanthanides has become an emerging field of research due to the potential environmental implications and biotechnological opportunities. In *Pseudomonas putida* KT2440, the two pyrroloquinoline quinone-dependent alcohol dehydrogenases PedE and PedH are inversely produced in response to La^{3+}-availability. This REE-switch is orchestrated by a complex regulatory network including the PedR2/PedS2 two-component system and is important for efficient growth on several alcoholic volatiles. As *P. putida* is exposed to a broad variety of organic compounds in its natural soil habitat, the cellular responses towards La^{3+} during growth on various model carbon sources were investigated with a differential proteomic approach. Apart from the Ca^{2+}-dependent enzyme PedE, the differential abundance of most other identified proteins was conditional and revealed a substrate specificity. Concomitant with the proteomic changes, La^{3+} had a beneficial effect on lag-phases while causing reduced growth rates and lower optical densities in stationary phase during growth on glycerol. When these growth phenotypes were evaluated with mutant strains, a novel metabolic route for glycerol utilization was identified that seems to be functional in parallel with the main degradation pathway encoded by the *glpFKRD* operon. The newly discovered route is initiated by PedE and/or PedH, which most likely convert glycerol to glyceraldehyde. In the presence of lanthanum, glyceraldehyde seems to be further oxidized to glycerate, which, upon phosphorylation to glycerate-2-phosphate by the glycerate kinase GarK, is finally channelled into the central metabolism.

45 ## Importance

46 The biological role of rare earth elements has long been underestimated and research has mainly
47 focused on methanotrophic bacteria thus far. We have recently demonstrated that *P. putida*, a plant
48 growth promoting bacterium that thrives in the rhizosphere of various feed crops, possesses a REE-
49 dependent alcohol dehydrogenase, but knowledge about lanthanide-dependent effects on
50 physiological traits in non-methylotrophic bacteria is still scarce. This study demonstrates that the
51 cellular response of *P. putida* KT2440 towards La^{3+} is mostly substrate specific and that during growth
52 on glycerol, La^{3+} has a severe effect on several growth parameters. We provide compelling evidence
53 that these changes are linked to glycerol oxidation by the La^{3+}-dependent alcohol dehydrogenase
54 PedH and thereby identify a novel route for glycerol metabolism in this organism. Overall, these
55 findings demonstrate that lanthanides can alter important physiological traits of non-methylotrophic
56 bacteria, which might consequently influence their competitiveness during colonization of various
57 environmental niches.

58 ## Introduction

59 The rhizosphere, defined as the narrow region of soil surrounding plant roots, is one of the most
60 complex ecosystems on earth containing a multitude of organisms from different taxa including
61 fungi, oomycetes, nematodes, protozoa, algae, viruses, archaea and arthropods as well as up to 10^8
62 soil dwelling bacteria per gram of fresh root (1–3). Its diversity is mainly shaped by root exudates, a
63 complex mixture of organic compounds including carbohydrates, amino acids, or carbon acids (4, 5)
64 and plant-, fungal-, and bacteria-derived volatiles (VOCs) such as alkenes, alcohols, terpenes or
65 benzenoids (6, 7). As such, it is not surprising that the soil-dwelling organism *P. putida* KT2440 is
66 equipped with a broad diversity of metabolic pathways in order to maximize its cellular fitness in
67 different environmental niches including the rhizosphere (8–10). For efficient growth on various
68 alcoholic VOC substrates, it uses a periplasmic oxidation system consisting of the pyrroloquinoline
69 quinone-dependent alcohol dehydrogenases (PQQ-ADHs) PedE and PedH (11, 12). The enzymes
70 appear to be functionally redundant but differ in their metal cofactor dependency. PedE is a Ca^{2+}-
71 dependent enzyme, whereas PedH requires the presence of rare earth elements (REEs) of the
72 lanthanide series (Ln^{3+}) for catalytic activity (12, 13).
73 Although being among the most ubiquitous metals in the earth's crust, REEs were long considered to
74 be of no biological relevance due to their low solubility under environmental conditions (14). Indeed,
75 the only known and characterized REE-dependent enzymes thus far belong to the family of PQQ-
76 ADHs of methano- and methylotrophic bacteria as well as the non-methylotrophic organism *P. putida*
77 KT2440 (12, 15–20). A characteristic aspartic acid that is additionally present in the metal
78 coordination sphere of these enzymes is associated with Ln^{3+}-binding. Notably, this specific amino
79 acid residue has been found in the genome of many bacteria from various origins indicating a broad
80 distribution of Ln^{3+}-dependent enzymes (21–25). Very recently, another Ln^{3+}-binding protein, called
81 lanmodulin, was identified in *M. extorquens* AM1 (26). This periplasmic protein, which shows
82 structural similarities with the Ca^{2+}-binding protein calmodulin, is able to bind up to four Ln^{3+} ions per
83 protein with picomolar affinity and changes its conformation from a largely disordered to a compact,

84 ordered state upon REE binding. Although its exact cellular role has yet to be established, it has been
85 speculated that it might play a role in Ln^{3+}-uptake. Further, homologous genes have only been
86 identified in the genome of some other species of *Methylobacteria* and *Bradyrhizobia*.
87 In addition to their functional role as metal cofactor, several studies have recently investigated the
88 effect of REEs on cellular physiology in different methano- and methylotrophic organisms (20, 27–
89 32). Some of these studies found different physiological traits to be influenced in response to Ln^{3+}-
90 availability including changes in metabolite cross feeding, growth rates and -yields, or biofilm
91 formation. It is further interesting to note that REEs have been used as micro-fertilizers, especially in
92 China, for over 30 years, as Ln^{3+}-supplementation can be associated with increased growth of
93 different food crops including rice, mungbean, maize, and coconut plants (33–37).
94 The aforementioned results suggest that apart from the inverse transcriptional regulation of PQQ-
95 ADHs, which has been described in detail for different organisms including *P. putida* (12, 19, 27, 38–
96 42), additional responses towards REEs exist and could depend on the specific organism and/or
97 environmental context. To investigate the existence of such conditional cellular responses in the non-
98 methylotrophic organism *P. putida* KT2440, we used a differential proteomic approach during growth
99 on various model carbon sources that reflect the metabolic diversity of the rhizosphere. From these
100 experiments, we found that the Ca^{2+}-dependent PQQ-ADH PedE was the only protein showing a
101 differential abundance during growth on all carbon sources tested. The vast majority of identified
102 proteins were differentially abundant only under one specific growth condition. During growth on
103 glycerol and 2-phenylethanol, which both represent substrates for PedE and PedH, a
104 disproportionally high number of metabolism related proteins were more abundant in the presence
105 of La^{3+}, while this was not the case during growth on citrate and glucose, substrates for which no
106 activity of these enzymes is observed. In addition, physiological characteristics, such as growth rates
107 and the lag-phase, of cultures could be linked to the differential activity pattern of PedE and PedH
108 during growth on glycerol. Based on these results, we were able to identify and reconstruct a novel
109 metabolic route for glycerol utilisation, which depends on PedE and/or PedH activity. This route
110 seems to operate in conjunction with the previously described major degradation pathway initiated

111 by the glycerol kinase GlpK and most likely ensures efficient growth of *P. putida* on this polyol

112 substrate.

113 ## Materials and Methods

114 *Bacterial strains, plasmids and culture conditions*

115 A complete list of all strains, plasmids, and primers used in this study can be found in **Table S1** and
116 **Table S2**. All *Pseudomonas putida* and *Escherichia coli* strains were maintained on solidified LB
117 medium (43). If necessary, 40 µg/mL kanamycin or 20 µg/mL 5-fluorouracil were added for
118 maintenance and/or selection. For growth, liquid LB medium or a modified M9 salt medium (12)
119 supplemented with 5 mM 2-phenylethanol, 25 mM succinate, 10 mM glucose, 10 mM citrate, 20 mM
120 DL-glycerate, or 20 mM glycerol as sole source of carbon and energy was used. If not stated
121 otherwise, precultures were grown overnight in test tubes with 3 ml M9 medium supplemented with
122 succinate at 30°C and 180 rpm. The next day, cells were washed twice with M9 medium without
123 supplemented C-source, and used to inoculate 200 µL of M9 medium supplemented with the desired
124 C-source in a 96-well microtiter plate (Falcon, product no. 353047 or Sarstedt, product no. 83.3924)
125 and incubated at 30°C and 250 rpm in a microplate reader (Xenius, Safas Monaco) or 28°C and 220
126 rpm in a rotary shaker (Forma, Thermo Scientific). Maximum growth rates (μ_{max}) and lag-times (λ)
127 were estimated based on fitting the natural logarithm of the relative OD_{600} values ($\ln(N/N_0)$, with N
128 being OD_{600} at time t) with the Richards growth model using the "grofit" package in R (44). As OD_{600}
129 decreased directly upon begin of the experiment, $\ln(N/N_{t=3\,h})$ was used instead of $\ln(N/N_0)$ for better
130 fit. Differences in lag-times, growth rates, and maximal OD_{600} during stationary phase (OD_{600}^{max}) were
131 evaluated by statistical analysis in GraphPad PRISM using a two-tailed *t*-test ($\alpha = 0.05$, $n = 3$).

132

133 *Construction of plasmids*

134 Deletion plasmids pJOE-calA, pJOE-garK, pJOE-glp, and pMW08 were constructed as follows: the 650-
135 bp to 1000-bp regions upstream and downstream of the *calA* (PP_2426), *garK* (PP_3178), *glpFKRD*
136 (PP_1076 to PP_1973), or *glcDEF* (PP_3745 to PP_3747) genes were amplified from genomic DNA of
137 *P. putida* KT2440 using primers PcalA1 to PcalA4, PgarK1 to PgarK4, Pglp1 to Pglp4, or MWH03 to

138 MWH06 (**Table S2**). The two up- and downstream fragments and BamHI-digested pJOE6261.2 were
139 then joined together using one-step isothermal assembly (45).
140
141 *Strain constructions*
142 Deletion mutant strains were constructed as previously described (46). Briefly, the integration vector
143 pJOE6261.2 harbouring the up- and downstream regions of the target gene(s) was transformed into
144 *P. putida* KT2440 *Δupp* (KT2440*). Kanamycin (Kan) resistant and 5-fluorouracil (5-FU) sensitive
145 clones were selected and one of these was incubated in LB medium at 30°C for 24 h. The cell
146 suspension was then plated on M9 minimal agar plates containing 25 mM succinate and 20 µg ml^{-1} 5-
147 FU. Clones that carried the desired gene deletion were identified by colony PCR of the 5-FU^r Kan^s
148 clones using primer pair PcalA1/PcalA4, PgarK1/PgarK4, Pglp1/Pglp4, or MWH03/MWH06.
149
150 *Protein extraction for comparative proteome analysis*
151 For comparative proteome analysis experiments, 50 ml M9 medium supplemented with citrate,
152 glucose, glycerol or 2-phenylethanol and 0 or 10 µM $LaCl_3$ were inoculated with an OD_{600} of 0.05 from
153 succinate precultures of strain *P. putida* KT2440* in 250 ml polycarbonate Erlenmeyer flasks and
154 incubated at 30°C and 180 rpm. When cell cultures reached an OD_{600} of > 0.4, cells were harvested by
155 centrifugation for 15 min at 6000 x g and 4°C. Cell pellets were resuspended in 1 ml sample buffer
156 (150 mM Tris-HCl pH 6.8; 2 % SDS; 20 mM dithiothreitol) and heated for 5 min at 95°C with gentle
157 shaking. Subsequently, samples were centrifuged for 15 min at 21000 x g and 4°C, and the
158 supernatants were stored in new reaction tubes at -20 °C. In a next step, proteins were precipitated
159 using chloroform-methanol (47) and pellets were resuspended in Tris-buffered (50 mM, pH 8.5) urea
160 (6 M). Protein concentrations were determined by the Bradford assay (48).
161
162 *In-solution digest of proteins and peptide purification with C18 Stage Tips*
163 To 25 µg protein in 60 µl Tris-buffered (50 mM, pH 8.5) urea (6 M), DTT was added to a final
164 concentration of 10 mM to guarantee reduction of cysteines. Samples were incubated for 30 min at

165 56 °C under shaking at 1000 rpm. Alkylation of cysteines was performed by adding 30 mM
166 iodoacetamide and incubation for 45 min at room temperature in the dark. Alkylation was stopped
167 by adding 50 mM DTT and samples were incubated for another 10 min at RT. 500 ng LysC protease
168 (Roche) in 50 mM Tris buffer (pH 8.5) was added and samples were digested overnight at 30 °C. Next,
169 the urea in the reaction mixture was diluted to 2 M by adding the appropriate amount of Tris buffer
170 (50 mM, pH 8.5). 1 µg trypsin (Roche) in Tris buffer (50 mM, pH 8.5) was added and digestion was
171 continued for 4 hours at 37 °C. The digest was stopped by addition of 3 µl 10% (v/v) trifluoroacetic
172 acid (TFA). Next, peptide mixtures were concentrated and desalted on C18 stage tips (49) and dried
173 under vacuum. Samples were dissolved in 20 µl 0.1% (v/v) TFA. Aliquots of 1 µl were subjected to
174 nanoLC-MS/MS analysis.
175
176 *Mass spectrometry analysis*
177 NanoLC-ESI-MS/MS experiments were performed on an EASY-nLC 1200 system (Thermo Fisher
178 Scientific) coupled to a Q-Exactive Plus mass spectrometer (Thermo Fisher Scientific) using an EASY-
179 Spray nanoelectrospray ion source (Thermo Fisher Scientific). Tryptic peptides were directly injected
180 to an EASY-Spray analytical column (2 µm, 100 Å PepMapRSLC C18, 25 cm × 75 µm, Thermo Fisher
181 Scientific) operated at constant temperature of 35 °C. Peptides were separated at a flow rate of 250
182 nL/min using a 240 min gradient with the following profile: 2% - 10% solvent B in 100 min, 10% - 22%
183 solvent B in 80 min, 22% - 45% solvent B in 55 min, 45% - 95% solvent B in 5 min and isocratic at 90%
184 solvent B for 15 min. Solvents used were 0.5 % acetic acid (solvent A) and 0.5% acetic acid in
185 acetonitrile/H2O (80/20, v/v, solvent B). The Q Exactive Plus was operated under the control of
186 XCalibur 3.0.63 software. MS spectra (m/z = 300-1600) were detected in the Orbitrap at a resolution
187 of 70000 (m/z = 200) using a maximum injection time (MIT) of 100 ms and an automatic gain control
188 (AGC) value of 1 x 10^6. Internal calibration of the Orbitrap analyzer was performed using lock-mass
189 ions from ambient air as described elsewhere (50). Data dependent MS/MS spectra were generated
190 for the 10 most abundant peptide precursors in the Orbitrap using high energy collision dissociation
191 (HCD) fragmentation at a resolution of 17500, a normalized collision energy of 27 and an intensity

192 threshold of 1.3 x 10^5. Only ions with charge states from +2 to +5 were selected for fragmentation
193 using an isolation width of 1.6 Da. For each MS/MS scan, the AGC was set at 5 x 10^5 and the MIT was
194 100 ms. Fragmented precursor ions were dynamically excluded for 30 s within a 5 ppm mass window
195 to avoid repeated fragmentation.
196
197 *Protein quantification and data analysis*
198 Raw files were imported into MaxQuant (51) version 1.6.0.1 for protein identification and label-free
199 quantification (LFQ) of proteins. Protein identification in MaxQuant was performed using the
200 database search engine Andromeda (52). MS spectra and MS/MS spectra were searched against *P.*
201 *putida* KT2440 protein sequence database downloaded from UniProt (53). Reversed sequences as
202 decoy database and common contaminant sequences were added automatically by MaxQuant. Mass
203 tolerances of 4.5 ppm (parts per million) for MS spectra and 20 ppm for MS/MS spectra were used.
204 Trypsin was specified as enzyme and two missed cleavages were allowed. Carbamidomethylation of
205 cysteines was set as a fixed modification and protein N-terminal acetylation and oxidation were
206 allowed as variable modifications. The 'match between runs' feature of MaxQuant was enabled with
207 a match time window of one minute and an alignment time window of 20 minutes. Peptide false
208 discovery rate (FDR) and protein FDR thresholds were set to 0.01.
209 Statistical analysis including *t*-tests and principal component analysis (PCA) were performed using
210 Perseus software version 1.6.0.2 (54). Matches to contaminant (e.g., keratins, trypsin) and reverse
211 databases identified by MaxQuant were excluded from further analysis. Proteins were considered for
212 LFQ (label free quantification) if they were identified by at least two peptides. First, normalized LFQ
213 values from MaxQuant were log2 transformed. Missing values were replaced from normal
214 distribution using a width of 0.2 and a downshift of 2.0. Statistical differences between two sample
215 groups were determined using an unpaired *t*-test and a p-value < 0.01 and a regulation factor > 2
216 (log2 fold-change > 1) were considered as significant change in protein abundance. The mass
217 spectrometry proteomics data will be deposited to the ProteomeXchange Consortium via the PRIDE
218 (55) partner repository (submitted).

219

220 *Purification and activity measurement of PQQ-ADHs PedE and PedH*

221 To measure the activity of the two PQQ-ADHs PedE and PedH, the enzymes were expressed in *E. coli*
222 BL21(DE3) cells using plasmids pMW09 and pMW10, and purified by affinity chromatography as
223 described elsewhere (12). The activities with the four substrates 2-phenylethanol, citrate, glucose
224 and glycerol were determined at a concentration of 10 mM using a previously described colorimetric
225 assay (12) with one minor modification. To represent the growth conditions, 1 µM La^{3+} instead of 1
226 µM Pr^{3+} was used as metal cofactor for PedH.

227

228 **Funding Information**

229 The work of Matthias Wehrmann and Janosch Klebensberger was supported by an individual
230 research grant from the Deutsche Forschungsgemeinschaft (DFG, KL 2340/2-1). The work of
231 Maxime Toussaint and Patrick Billard was supported in part by Labex Ressources21 (ANR-10-
232 LABX-21-01).

233

234 **Acknowledgements**

235 The authors would like to thank Prof. Bernhard Hauer for his continuous support. The
236 authors further declare that the research was conducted in the absence of any commercial
237 or financial relationships that could be construed as a potential conflict of interest.

238 ## Results

239 We have recently demonstrated that the two PQQ-dependent ADHs PedE and PedH are inversely
240 regulated dependent on the presence of rare earth elements (REEs) and that a complex signalling
241 network that includes the activity of the PedR2/PedS2 two-component system orchestrates this
242 regulation (12, 38). In order to identify whether a global cellular response of *P. putida* KT2440
243 towards REEs beyond the regulation of the PQQ-ADHs exists, we used a comparative proteomic
244 analysis during growth on four different carbon and energy sources, namely 2-phenylethanol,
245 glycerol, glucose, and citrate.

246

247 *Evaluation of proteomics data*

248 Proteins were extracted from cells of *P. putida* by SDS to enable extraction of cytoplasmic as well as
249 transmembrane proteins followed by label free nano-LC-MS/MS quantification. In total, 2771
250 proteins with at least two unique peptides and an FDR ≤ 1% were identified and quantified by our
251 proteomics approach, corresponding to 50% of the *P. putida* KT2440 proteome. Principal component
252 analysis revealed high reproducibility for sample replicates and distinct patterns for the different
253 carbon sources (**Fig. S1**). The majority of proteins was increased or decreased in abundance in
254 response to the different carbon sources. In contrast, minor differences were observed in the
255 presence or absence of La^{3+} during growth on the same carbon source. Proteins that exhibited a 2-
256 fold or higher change in abundance between different growth conditions and a *p*-value ≤ 0.01 were
257 considered as differentially abundant.

258

259 *Effect of lanthanum on protein abundance during growth with different substrates*

260 According to the aforementioned criteria, 56 proteins were identified as differentially abundant
261 comparing growing cells of *P. putida* in the presence and absence of La^{3+} with different carbon
262 sources (**Fig. 1, Table 3, Table S3-S5**). In these studies, only the Ca^{2+}-dependent PQQ-ADH PedE
263 (PP_2674) showed a decreased abundance in response to La^{3+} during growth on all four different

264 carbon and energy substrates. The Ln^{3+}-dependent PQQ-ADH PedH (PP_2679) showed an increased
265 abundance in response to La^{3+} during growth on glucose, glycerol, and 2-phenylethanol, whereas an
266 uncharacterized pentapeptide repeat containing protein (PP_2673) that is directly upstream of *pedE*
267 showed a decreased abundance during growth on glycerol and 2-phenylethanol (**Fig. 1**). The
268 remaining 53 proteins were only identified under one specific growth condition (**Table 3, Table S3-**
269 **S5**).
270 During growth on 2-phenylethanol and glycerol, a majority of the identified proteins was increased in
271 abundance (80% and 70%) in response to La^{3+} (**Table 3, Table S3**). For glucose and citrate this was
272 different, as most of the identified proteins were found to be less abundant in response to La^{3+} (36%
273 and 40% during growth on glucose and citrate; **Table S4 and Table S5**). Notably, the majority of the
274 identified proteins were related to metabolism according to the cluster of orthologous protein
275 groups (COG) database (56). To test whether the observed conditional proteomic response is linked
276 to PedE and/or PedH activity, we determined the corresponding enzyme activities with all four
277 carbon and energy sources (**Table 1**). Apart from the already known substrate 2-phenylethanol, PedE
278 and PedH also showed activity with glycerol, whereas no activity could be detected with citrate or
279 glucose.
280
281 *Effect of lanthanum during growth on glycerol*
282 From our proteomic- and biochemical data, we wondered whether PedE and PedH activity could play
283 a beneficial role during glycerol metabolism of *P. putida* KT2440. As the degradation pathway and
284 growth characteristics of this organism have been recently characterized in great detail (57, 58), we
285 wanted to have a closer look on the effect of La^{3+} during growth on this specific substrate. In these
286 experiments (**Fig. 2A, Table 2)**, we consistently observed a shorter lag-phase (λ) of the cultures in
287 response to La^{3+} availability (10.2 ± 0.2 h vs. 17.3 ± 0.2). Additionally, the corresponding values of the
288 specific growth rates (μ_{max}, 0.201 ± 0.004 vs. 0.341 ± 0.010 h^{-1}) and the maximal OD_{600} in stationary
289 phase (OD_{600}^{max}; 0.680 ± 0.014 vs. 0.884 ± 0.004) of the cultures also differed in the presence or
290 absence of La^{3+}, respectively. As the purified PedH enzyme showed an 3-fold higher specific activity

291 towards glycerol compared to PedE *in vitro* (0.9 ± 0.1 U mg^{-1} vs. 0.3 ± 0.1 U mg^{-1}; **Table 1**), we
292 speculated that this increased glycerol conversion by PedH could be the underlying cause for the
293 observed differences in growth parameters. When subsequently a Δ*pedE* Δ*pedH* strain was analysed
294 for growth in the presence and absence of La^{3+} (**Fig. 2B**, **Table 2**), no significant differences in λ and
295 μ_{max} were observed for the Δ*pedE* Δ*pedH* strain in response to La^{3+} while, although less profound,
296 small differences in OD_{600}^{max} were still detected. Further, we found that under both conditions the
297 double deletion strain showed a lag-phase that was undistinguishable from that of the parental strain
298 in the absence of La^{3+} but dramatically longer than that of the parental strain in the presence of La^{3+}
299 (17.5 ± 0.3 h in the absence of La^{3+} and 17.2 ± 0.4 h in the presence of 10 µM La^{3+}). Interestingly, the
300 growth rates under both conditions (0.276 ± 0.008 h^{-1} and 0.291 ± 0.012 h^{-1}) were significantly higher
301 ($p < 0.01$) than those of the parental strain in presence of La^{3+} while still being significantly below ($p <$
302 0.05) those of the parental strain in the absence of La^{3+}.
303 These results implied that the two PQQ-ADHs can indeed be beneficial for growth on glycerol and
304 that a functionally active PedH enzyme is the underlying cause for the La^{3+}-dependent differences in
305 lag-times and growth rates and to some extent also for differences in OD_{600}^{max} of KT2440 cultures. As
306 PedE and PedH as well as the remaining proteins that were found to be differentially abundant in
307 response to La^{3+} during growth on glycerol, are not part of the described degradation pathway in *P.*
308 *putida* KT2440 (57, 58), we hypothesized that an additional metabolic route exists (**Fig. 3**). Based on
309 our proteomic data, this route could be initiated by the activity of PedH and the oxidation of glycerol
310 to glycolaldehyde. In the next steps glycolaldehyde could be oxidized to glycerate by PedH, the
311 aldehyde dehydrogenase AldB-II, or the aldehyde oxidase complex composed of proteins PP_3621
312 (IorA-II), PP_3622 and PP_3623 (AdhB). After phosphorylation by the glycerate kinase GarK,
313 glycerate-2-phosphate could eventually enter the central metabolism.
314 If such a metabolic route exists, a Δ*glpFKRD* deletion strain should still be able to grow with glycerol
315 as sole source of energy and carbon, whereas a Δ*pedE* Δ*pedH* Δ*glpFKRD* deletion mutant should not.
316 To test this scenario, the corresponding strains were constructed and characterized for their growth
317 phenotypes (**Fig. 4A**). We found that *P. putida* KT2440 indeed grew on glycerol independent of the

318 *glp* regulon, although growth was dramatically impaired compared to the parental strain or strain
319 Δ*pedE* Δ*pedH*. When PedE and PedH were additionally deleted, growth could not be observed even
320 after a prolonged incubation time of 5 d. This supported our hypothesis that a metabolic route for
321 glycerol next to the *glp* pathway exists and that this route is initiated by the PedE and PedH proteins,
322 most likely by the oxidation of glycerol to glyceraldehyde (**Fig. 3**). Given that the route further
323 proceeds via glycerate and glycerate-2-phosphate, different cellular concentrations of these
324 metabolites would be expected during growth on glycerol in a mutant that is not able to use the *glp*
325 pathway. Interestingly, a companion study to this work employed a metabolome analysis using
326 glycerol-growing cells of *P. putida* KT2440 and a Δ*glpK* deletion strain, which can only use the
327 proposed novel route via PedE and PedH (59). In their experiments, the authors observed that the
328 glycerate concentration measured for the Δ*glpK* strain was dramatically increased compared to the
329 wild type, whereas concentrations of glyceraldehyde and glyceraldehyde-3-phosphate were in the
330 same range for both strains. These data suggested that glycerate is indeed an intermediate during
331 *glp*-independent growth, and that the activity of downstream proteins represent the bottleneck of
332 the metabolic route leading to the observed accumulation. As our proteomic data indicated the
333 involvement of the predicted glycerate kinase GarK, we constructed a Δ*garK* deletion strain and
334 speculated that this strain should lack the ability to phosphorylate glycerate and would hence be
335 incapable of channelling glycerate-2-phosphate into the central metabolism. We indeed observed no
336 growth of a Δ*garK* mutant on glycerate even after incubation of up to 5 d, while strain Δ*pedE* Δ*pedH*
337 Δ*glpFKRD* could grow and reached OD_{600}^{max} within 72 h of incubation under the condition tested (**Fig.**
338 **4B**).
339 When grown on glycerol, no significant effect on growth rates and lag-times as well as only a minor,
340 but significant, negative effect on the OD_{600}^{max} ($p < 0.01$) was observed for the Δ*garK* deletion in the
341 absence of La^{3+}. In contrast, the same deletion caused a dramatic growth impairment in the presence
342 of La^{3+} (**Fig. 5A**, **Table 2**) and consequently the stationary phase was not reached during the 40 h of
343 incubation. Hence, no reliable growth parameter could be deduced from these data. It is however
344 obvious that the growth rate was far below the one of the parental strain in the presence of La^{3+}.

345 Notably, some of the most severely upregulated proteins in response to La^{3+} can either be associated
346 with stress responses, namely the multidrug efflux pump MexEF and the alkylhydroperoxide
347 reductase subunits AhpC/F, or enzymes, which play no obvious roles within the proposed metabolic
348 route, such as CalA, a predicted coniferyl alcohol dehydrogenase, and the glycolate oxidase GlcDEF.
349 Nevertheless, to test the potential metabolic influence of the latter two enzymes, we constructed
350 and analysed the corresponding Δ*calA* and Δ*glcDEF* mutants and tested their growth pattern with
351 glycerol (**Fig. 5B; Table 2**). The Δ*glcDEF* mutants showed a similar growth behaviour than the parental
352 strain. In contrast, strain Δ*calA* exhibited a significantly increased growth rate ($p < 0.01$) and higher
353 OD_{600}^{max} ($p < 0.01$) than the parental strain in the presence of La^{3+} while showing no significant
354 differences in OD_{600}^{max} and maximal growth rate and only minor differences ($p < 0.05$) in lag-times in
355 the absence of La^{3+}(**Fig. 5C; Table 2**).

356 ## Discussion

357 In the present study, the cellular responses of the soil bacterium *P. putida* KT2440 towards La^{3+}
358 availability during growth on several carbon and energy sources were investigated. The only protein
359 that showed a differential abundance independent of the substrate used for growth was the Ca^{2+}-
360 dependent PQQ-ADH PedE. This result is in line with data from a previous study (38), which
361 demonstrated that the La^{3+}-induced downregulation of *pedE* is dependent on the PedS2/PedR2 two-
362 component system that, based on our current observation, seems to be functional under all tested
363 conditions. The other two proteins that showed differential abundance under more than one culture
364 condition (PedH, PP_2673) are both also part of the *ped* gene cluster. Notably, the carbon sources
365 under which these proteins were identified either represent substrates of the two PQQ-ADHs PedE
366 and PedH, or can be degraded by an enzyme depending on the same PQQ-cofactor, namely the
367 glucose dehydrogenase Gcd. The remaining 53 proteins that showed differential abundance in
368 response to La^{3+} were identified only during growth on one substrate, suggesting a conditional
369 regulation. For glycerol, we provide striking evidence that the increased activity of PedH compared to
370 PedE is the primary cause for the observed proteomic and physiological changes during growth.
371 Thus far, the degradation of glycerol was described to start by the uptake *via* GlpF, phosphorylation
372 by GlpK, and subsequent GlpD-catalysed oxidation of glycerol-3-phosphate to dihydroxyacetone-3-
373 phosphate (58). In a next step, dihydroxyacetone-3-phosphate is interconverted to glyceraldehyde-3-
374 phosphate and enters the central metabolism. This pathway is negatively regulated by the
375 transcriptional regulator GlpR, and the de-repression of the *glpFKRD* operon is believed to depend on
376 the intracellular concentration of glycerol-3-phosphate, which finally impacts the lag-phase of
377 cultures (57). As such, it was interesting to find that growth on glycerol in the presence of La^{3+} led to
378 a shorter lag phase and lower growth rate of the parent strain, and that a Δ*pedE* Δ*pedH* mutant
379 showed a lag-phase similar to the parent in absence of La^{3+} without any beneficial effect of La^{3+} while
380 still growing with a higher growth rate than the parent strain in presence of La^{3+}. Further experiments
381 revealed that a Δ*glpFKRD* deletion strain is still able to grow on glycerol, while a Δ*pedE* Δ*pedH*

382 Δ*glpFKRD* is not. With the additional observation that a Δ*garK* mutant cannot utilize glycerate, we
383 propose a novel route for glycerol metabolism, in which PedE and PedH catalyse the initial oxidation
384 of glycerol to glyceraldehyde. In the presence of La^{3+}, the route seems to proceed via a second
385 oxidation step to glycerate, which is subsequently converted to glycerate-2-phosphate by the activity
386 of GarK (**Fig. 3**). Our data suggest that the PedE/PedH-dependent route, despite being important for
387 efficient growth, is not the main route for glycerol metabolism, as the effect of the Δ*pedE* Δ*pedH*
388 deletion on the lag-phase with glycerol is far less severe than deletion of the *glpFKRD* gene cluster. It
389 also appears that the PedE/PedH-dependent route is less efficient than the *glp* pathway, as the
390 overall growth of the Δ*glpFKRD* strain is substantially impaired compared to the Δ*pedE* Δ*pedH* strain.
391 A possible explanation for these observations could be the formation of the toxic intermediate
392 glyceraldehyde, which is known for its protein crosslinking properties and the formation of
393 superoxide radicals due to auto-oxidation (60, 61). The observed differences in growth rates and
394 OD_{600}^{max} in response to La^{3+} in the parent strain would thus reflect the increased metabolic flux
395 towards glyceraldehyde due to the higher specific activity of PedH compared to PedE. This would
396 also explain the severe La^{3+}-dependent growth impairment of the Δ*garK* mutant, as one can assume
397 that even higher concentrations of glyceraldehyde accumulate in a mutant that cannot process
398 glycerate. The notion that the MexEF RND transporter proteins, which are involved in efflux of
399 various toxic compounds (62), and the hydroyperoxide reductase proteins AhpC and AhpF, which
400 have been linked to ROS detoxification in *P. putida* (63), were also more abundant in presence of La^{3+}
401 during growth on glycerol are supportive of such a hypothesis.
402 To explain the impact of La^{3+} on the lag-times of cultures, one could speculate that in addition to
403 glycerol-3-phosphate, also other phosphorylated derivatives, such as glycerate-2-phosphate, are able
404 to relieve the repression of *glpFKRD* by GlpR. However, as in the absence of La^{3+} the growth
405 phenotype of the Δ*garK* mutant is indistinguishable from that of the parental strain, and since the
406 growth rate of the parent strain in absence of La^{3+} is still significantly higher than the growth rate of
407 strain Δ*pedE* Δ*pedH,* we postulate that yet another metabolic route is present that contributes to
408 growth without affecting the lag-phase. This route could proceed via the phosphorylation of

409 glyceraldehyde to glyceraldehyde-3-phosphate by the activity of a so-far unknown kinase. Whether
410 both alternative routes to the *glp*-dependent pathway are functional in parallel or whether the
411 metabolic flux *via* glycerate is exclusively induced in the presence of La^{3+} is currently unknown and
412 would need to be tested in future studies.

413 Similarly, the question why proteins that cannot be associated to the predicted glycerol metabolism
414 pathways are among the most differentially abundant proteins in response to La^{3+} remains to be
415 elucidated. It is however worthwhile noting that the two enzymes CalA and GlcDEF are either known,
416 (GlcDEF) or predicted by the PROSITE software tool (CalA) (64) to be catalytically active on 2-hydroxy
417 acids. As such, activity towards pathway intermediates such as glycerate cannot be excluded at the
418 moment.

419 From our data, the La^{3+}-dependent proteomic and physiological changes during growth on glycerol
420 can be explained by a shift in metabolic flux resulting from differences in the specific enzyme
421 activities between PedH and PedE. A similar metabolic-driven interpretation can also be used to
422 explain the differences observed during growth on other carbon and energy sources that are known
423 to be substrates for PedE and PedH such as 2-phenylethanol. However, this logic clearly fails to
424 explain the conditional differences during growth on glucose and citrate, as they do not represent
425 substrates for PedE and/or PedH. Despite the fact that we currently do not know the underlying
426 cause for conditional regulation under these conditions, it indicates that beside the interaction with
427 PedH and the TCS PedS2/PedR2, additional effects of REEs in *P. putida* do exist. Such effects could
428 include the inhibition of protein functions by mismetallation (65, 66), changes in the physiology of
429 the outer membrane (67), or so far unknown REE-dependent enzymes and regulator proteins. The
430 latter explanation is of particular interest, as two recent studies provide strong evidence that specific
431 import systems that can transport Ln^{3+} into the cytoplasm of methylotrophic bacteria do exist (41,
432 68).

433 Altogether, the current study demonstrates that the utilization of REEs can influence important
434 physiological traits of *P. putida*, which could be highly beneficial in competitive environmental niches
435 such as the rhizosphere. The previously reported fertilizing effect of REEs on different food crops

436 could hence be the result of increased competitiveness of plant growth promoting organisms such as
437 *P. putida* during root colonization. This hypothesis is further supported by a recent study, which
438 found that Pseudomonads predominantly thrive on root exudates *in vivo* and are hence enriched in
439 the rhizosphere of *Arabidopsis thaliana* (10). As such, it will be interesting to see what future
440 research will add to the currently emerging theme of REEs being an important micronutrient for
441 methylotrophic and non-methylotrophic organisms.

442 **Reference**

443 1. Mendes R, Garbeva P, Raaijmakers J. 2013. The rhizosphere microbiome: significance of plant
444 beneficial, plant pathogenic, and human pathogenic microorganisms. FEMS Microbiol Rev
445 37:634–663.
446 2. Raaijmakers J, Paulitz TC, Steinberg C, Alabouvette C, Moënne-Loccoz Y. 2009. The
447 rhizosphere: a playground and battlefield for soilborne pathogens and beneficial
448 microorganisms. Plant Soil 321:341–361.
449 3. Berg G, Roskot N, Steidle A, Eberl L, Zock A, Smalla K. 2002. Plant-Dependent Genotypic and
450 Phenotypic Diversity of Antagonistic Rhizobacteria Isolated from Different *Verticillium* Host
451 Plants Plants. Appl Environ Microbiol 68:3328–3338.
452 4. Carvalhais LC, Dennis PG, Fedoseyenko D, Hajirezaei MR, Borriss R, Von Wirén N. 2011. Root
453 exudation of sugars, amino acids, and organic acids by maize as affected by nitrogen,
454 phosphorus, potassium, and iron deficiency. J Plant Nutr Soil Sci 174:3–11.
455 5. Dakora FD, Phillips DA. 2002. Root exudates as mediators of mineral acquisition in low-
456 nutrient environments. Plant Soil 245:35–47.
457 6. Schmidt R, Cordovez V, de Boer W, Raaijmakers J, Garbeva P. 2015. Volatile affairs in
458 microbial interactions. ISME J 9:2329–2335.
459 7. Insam H, Seewald MSA. 2010. Volatile organic compounds (VOCs) in soils. Biol Fertil Soils
460 46:199–213.
461 8. Wackett LP. 2003. *Pseudomonas putida*—a versatile biocatalyst. Nat Biotechnol 21:136–138.
462 9. Nelson KE, Weinel C, Paulsen IT, Dodson RJ, Hilbert H, Martins dos Santos VAP, Fouts DE, Gill
463 SR, Pop M, Holmes M, Brinkac L, Beanan M, DeBoy RT, Daugherty S, Kolonay J, Madupu R,
464 Nelson W, White O, Peterson J, Khouri H, Hance I, Lee PC, Holtzapple E, Scanlan D, Tran K,
465 Moazzez A, Utterback T, Rizzo M, Lee K, Kosack D, Moestl D, Wedler H, Lauber J, Stjepandic D,
466 Hoheisel J, Straetz M, Heim S, Kiewitz C, Eisen J, Timmis KN, Dusterhoft A, Tummler B, Fraser
467 CM. 2002. Complete genome sequence and comparative analysis of the metabolically
468 versatile *Pseudomonas putida* KT2440. Environ Microbiol 4:799–808.

469 10. Worsley SF, Macey MC, Newitt JT, Patrick E, Yu DW, Wilkinson B, Murrell C, Hutchings MI.
470 2019. Investigating the role of exudates in recruiting Streptomyces bacteria to the *Arabidopsis*
471 *thaliana* root microbiome. bioRxiv 532309.
472 11. Mückschel B, Simon O, Klebensberger J, Graf N, Rosche B, Altenbuchner J, Pfannstiel J, Huber
473 A, Hauer B. 2012. Ethylene glycol metabolism by *Pseudomonas putida*. Appl Environ Microbiol
474 78:8531–9.
475 12. Wehrmann M, Billard P, Martin-Meriadec A, Zegeye A, Klebensberger J. 2017. Functional Role
476 of Lanthanides in Enzymatic Activity and Transcriptional Regulation of Pyrroloquinoline
477 Quinone-Dependent Alcohol Dehydrogenases in *Pseudomonas putida* KT2440. MBio
478 8:e00570-17.
479 13. Takeda K, Matsumura H, Ishida T, Samejima M, Igarashi K, Nakamura N, Ohno H. 2013. The
480 two-step electrochemical oxidation of alcohols using a novel recombinant PQQ alcohol
481 dehydrogenase as a catalyst for a bioanode. Bioelectrochemistry 94:75–78.
482 14. Firsching FH, Brune SN. 1991. Solubility products of the trivalent rare-earth phosphates. J
483 Chem Eng Data 36:93–95.
484 15. Pol A, Barends TRM, Dietl A, Khadem AF, Eygensteyn J, Jetten MSM, Op den Camp HJM. 2014.
485 Rare earth metals are essential for methanotrophic life in volcanic mudpots. Environ
486 Microbiol 16:255–264.
487 16. Hibi Y, Asai K, Arafuka H, Hamajima M, Iwama T, Kawai K. 2011. Molecular structure of La^{3+}-
488 induced methanol dehydrogenase-like protein in *Methylobacterium radiotolerans*. J Biosci
489 Bioeng 111:547–549.
490 17. Fitriyanto NA, Fushimi M, Matsunaga M, Pertiwiningrum A, Iwama T, Kawai K. 2011.
491 Molecular structure and gene analysis of Ce^{3+}-induced methanol dehydrogenase of
492 *Bradyrhizobium* sp. MAFF211645. J Biosci Bioeng 111:613–617.
493 18. Good NM, Vu HN, Suriano CJ, Subuyuj GA, Skovran E, Martinez-Gomez NC. 2016.
494 Pyrroloquinoline Quinone Ethanol Dehydrogenase in *Methylobacterium extorquens* AM1
495 Extends Lanthanide-Dependent Metabolism to Multicarbon Substrates. J Bacteriol 198:3109–

496 3118.
497 19. Vu HN, Subuyuj GA, Vijayakumar S, Good NM, Martinez-Gomez NC, Skovran E. 2016.
498 Lanthanide-Dependent Regulation of Methanol Oxidation Systems in *Methylobacterium*
499 *extorquens* AM1 and Their Contribution to Methanol Growth. J Bacteriol 198:1250–1259.
500 20. Masuda S, Suzuki Y, Fujitani Y, Mitsui R, Nakagawa T, Shintani M, Tani A. 2018. Lanthanide-
501 Dependent Regulation of Methylotrophy in *Methylobacterium aquaticum* Strain 22A.
502 mSphere 3:e00462-17.
503 21. Chistoserdova L. 2016. Lanthanides: New life metals? World J Microbiol Biotechnol 32:138.
504 22. Keltjens JT, Pol A, Reimann J, Op den Camp HJM. 2014. PQQ-dependent methanol
505 dehydrogenases: rare-earth elements make a difference. Appl Microbiol Biotechnol 98:6163–
506 83.
507 23. Sowell SM, Abraham PE, Shah M, Verberkmoes NC, Smith DP, Barofsky DF, Giovannoni SJ.
508 2011. Environmental proteomics of microbial plankton in a highly productive coastal
509 upwelling system. ISME J 5:856–865.
510 24. Taubert M, Grob C, Howat AM, Burns OJ, Dixon JL, Chen Y, Murrell JC. 2015. XoxF encoding an
511 alternative methanol dehydrogenase is widespread in coastal marine environments. Environ
512 Microbiol 17:3937–3948.
513 25. Lv H, Sahin N, Tani A. 2018. Isolation and genomic characterization of *Novimethylophilus*
514 *kurashikiensis* gen. nov. sp. nov., a new lanthanide-dependent methylotrophic species of
515 Methylophilaceae. Environ Microbiol 20:1204–1223.
516 26. Cotruvo JA, Featherston ER, Mattocks JA, Ho J V, Laremore TN. 2018. Lanmodulin: A Highly
517 Selective Lanthanide-Binding Protein from a Lanthanide-Utilizing Bacterium. J Am Chem Soc
518 jacs.8b09842.
519 27. Gu W, Semrau JD. 2017. Copper and cerium-regulated gene expression in *Methylosinus*
520 *trichosporium* OB3b. Appl Microbiol Biotechnol 101:8499–8516.
521 28. Good NM, Walser ON, Moore RS, Suriano CJ, Huff AF, Cecilia N. 2018. Investigation of
522 lanthanide-dependent methylotrophy uncovers complementary roles for alcohol

523 dehydrogenase enzymes.
524 29. Fitriyanto NA, Nakamura M, Muto S, Kato K, Yabe T, Iwama T, Kawai K, Pertiwiningrum A.
525 2011. Ce^{3+}-induced exopolysaccharide production by *Bradyrhizobium* sp. MAFF211645. J
526 Biosci Bioeng 111:146–152.
527 30. Zheng Y, Huang J, Zhao F, Chistoserdova L. 2018. Physiological Effect of XoxG(4) on
528 Lanthanide-Dependent Methanotrophy. MBio 9:e02430-17.
529 31. Krause SMB, Johnson T, Samadhi Karunaratne Y, Fu Y, Beck DAC, Chistoserdova L, Lidstrom
530 ME. 2017. Lanthanide-dependent cross-feeding of methane-derived carbon is linked by
531 microbial community interactions. Proc Natl Acad Sci 114:358–363.
532 32. Akberdin IR, Collins DA, Hamilton R, Oshchepkov DY, Shukla AK, Nicora CD, Nakayasu ES,
533 Adkins JN, Kalyuzhnaya MG. 2018. Rare Earth Elements Alter Redox Balance in
534 *Methylomicrobium alcaliphilum* 20ZR. Front Microbiol 9:1–12.
535 33. Diatloff E, Smith FW, Asher CJ. 1995. Rare earth elements and plant growth: III. Responses of
536 corn and mungbean to low concentrations of cerium in dilute, continuously flowing nutrient
537 solutions. J Plant Nutr 18:1991–2003.
538 34. Diatloff E, Asher CJ, Smith FW. 1996. Rare earth elements and plant growth. Proc 8th Aust
539 Agron Conf Toowoomba, Queensland, Aust 30 January-2 February, 1996 3–6.
540 35. Pang X, Li D, Peng A. 2002. Application of rare-earth elements in the agriculture of China and
541 its environmental behavior in soil. Environ Sci Pollut Res 9:143–148.
542 36. Wahid PA, Valiathan MS, Kamalam N V., Eapen JT, Vijayalakshmi S, Prabhu RK, Mahalingam
543 TR. 2000. Effect of rare earth elements on growth and nutrition of coconut palm and root
544 competition for these elements between the palm and *calotropis gigantea*. J Plant Nutr
545 23:329–338.
546 37. Xie ZB, Zhu JG, Chu HY, Zhang YL, Zeng Q, Ma HL, Cao ZH. 2002. Effect of lanthanum on rice
547 production, nutrient uptake, and distribution. J Plant Nutr 25:2315–2331.
548 38. Wehrmann M, Berthelot C, Billard P, Klebensberger J. 2018. The PedS2/PedR2 Two-
549 Component System Is Crucial for the Rare Earth Element Switch in *Pseudomonas putida*

550 KT2440. mSphere 3:1–12.

551 39. Farhan Ul Haque M, Kalidass B, Bandow N, Turpin EA, DiSpirito AA, Semrau JD. 2015. Cerium
552 Regulates Expression of Alternative Methanol Dehydrogenases in *Methylosinus trichosporium*
553 OB3b. Appl Environ Microbiol 81:7546–7552.

554 40. Chu F, Beck DAC, Lidstrom ME. 2016. MxaY regulates the lanthanide-mediated methanol
555 dehydrogenase switch in *Methylomicrobium buryatense*. PeerJ 4:e2435.

556 41. Ochsner AM, Hemmerle L, Vonderach T, Nüssli R, Bortfeld-Miller M, Hattendorf B, Vorholt JA.
557 2019. Use of rare-earth elements in the phyllosphere colonizer *Methylobacterium extorquens*
558 PA1. Mol Microbiol 0–2.

559 42. Chu F, Lidstrom ME. 2016. XoxF Acts as the Predominant Methanol Dehydrogenase in the
560 Type I Methanotroph *Methylomicrobium buryatense*. J Bacteriol 198:1317–1325.

561 43. Maniatis T, Fritsch E, Sambrook J, Laboratory CSH. 1982. Molecular Cloning: A Laboratory
562 Manual. Cold Spring Harbor, N.Y. Cold Spring Harbor Laboratory.

563 44. Kahm M, Kschischo M, Ludwig J, Lichtenberg-Fraté H, Hasenbrink G. 2015. grofit: Fitting
564 Biological Growth Curves with R . J Stat Softw 33.

565 45. Gibson DG. 2011. Enzymatic Assembly of Overlapping DNA Fragments, p. 349–361. *In*
566 Methods in Enzymology.

567 46. Graf N, Altenbuchner J. 2011. Development of a method for markerless gene deletion in
568 *Pseudomonas putida*. Appl Environ Microbiol 77:5549–5552.

569 47. Wessel D, Flügge UI. 1984. A method for the quantitative recovery of protein in dilute solution
570 in the presence of detergents and lipids. Anal Biochem 138:141–143.

571 48. Bradford MM. 1976. A rapid and sensitive method for the quantitation of microgram
572 quantities of protein utilizing the principle of protein-dye binding. Anal Biochem 72:248–254.

573 49. Rappsilber J, Ishihama Y, Mann M. 2003. Stop and Go Extraction Tips for Matrix-Assisted Laser
574 Desorption/Ionization, Nanoelectrospray, and LC/MS Sample Pretreatment in Proteomics.
575 Anal Chem 75:663–670.

576 50. de Godoy LMF, Mortensen P, Makarov A, Li G, Macek B, Horning S, Pesch R, Mann M, Olsen J

577 V., Lange O. 2005. Parts per Million Mass Accuracy on an Orbitrap Mass Spectrometer via Lock
578 Mass Injection into a C-trap. Mol Cell Proteomics 4:2010–2021.
579 51. Cox J, Mann M. 2008. MaxQuant enables high peptide identification rates, individualized
580 p.p.b.-range mass accuracies and proteome-wide protein quantification. Nat Biotechnol
581 26:1367–1372.
582 52. Cox J, Neuhauser N, Michalski A, Scheltema RA, Olsen J V., Mann M. 2011. Andromeda: A
583 Peptide Search Engine Integrated into the MaxQuant Environment. J Proteome Res 10:1794–
584 1805.
585 53. Bateman A, Martin MJ, O'Donovan C, Magrane M, Alpi E, Antunes R, Bely B, Bingley M, Bonilla
586 C, Britto R, Bursteinas B, Bye-AJee H, Cowley A, Da Silva A, De Giorgi M, Dogan T, Fazzini F,
587 Castro LG, Figueira L, Garmiri P, Georghiou G, Gonzalez D, Hatton-Ellis E, Li W, Liu W, Lopez R,
588 Luo J, Lussi Y, MacDougall A, Nightingale A, Palka B, Pichler K, Poggioli D, Pundir S, Pureza L, Qi
589 G, Rosanoff S, Saidi R, Sawford T, Shypitsyna A, Speretta E, Turner E, Tyagi N, Volynkin V,
590 Wardell T, Warner K, Watkins X, Zaru R, Zellner H, Xenarios I, Bougueleret L, Bridge A, Poux S,
591 Redaschi N, Aimo L, ArgoudPuy G, Auchincloss A, Axelsen K, Bansal P, Baratin D, Blatter MC,
592 Boeckmann B, Bolleman J, Boutet E, Breuza L, Casal-Casas C, De Castro E, Coudert E, Cuche B,
593 Doche M, Dornevil D, Duvaud S, Estreicher A, Famiglietti L, Feuermann M, Gasteiger E, Gehant
594 S, Gerritsen V, Gos A, Gruaz-Gumowski N, Hinz U, Hulo C, Jungo F, Keller G, Lara V, Lemercier
595 P, Lieberherr D, Lombardot T, Martin X, Masson P, Morgat A, Neto T, Nouspikel N, Paesano S,
596 Pedruzzi I, Pilbout S, Pozzato M, Pruess M, Rivoire C, Roechert B, Schneider M, Sigrist C,
597 Sonesson K, Staehli S, Stutz A, Sundaram S, Tognolli M, Verbregue L, Veuthey AL, Wu CH,
598 Arighi CN, Arminski L, Chen C, Chen Y, Garavelli JS, Huang H, Laiho K, McGarvey P, Natale DA,
599 Ross K, Vinayaka CR, Wang Q, Wang Y, Yeh LS, Zhang J. 2017. UniProt: the universal protein
600 knowledgebase. Nucleic Acids Res 45:D158–D169.
601 54. Tyanova S, Temu T, Sinitcyn P, Carlson A, Hein MY, Geiger T, Mann M, Cox J. 2016. The
602 Perseus computational platform for comprehensive analysis of (prote)omics data. Nat
603 Methods 13:731–740.

604 55. Vizcaíno JA, Csordas A, Del-Toro N, Dianes JA, Griss J, Lavidas I, Mayer G, Perez-Riverol Y,
605 Reisinger F, Ternent T, Xu Q-W, Wang R, Hermjakob H. 2016. 2016 update of the PRIDE
606 database and its related tools. Nucleic Acids Res 44:D447–D456.
607 56. Galperin MY, Makarova KS, Wolf YI, Koonin E V. 2015. Expanded microbial genome coverage
608 and improved protein family annotation in the COG database. Nucleic Acids Res 43:D261–
609 D269.
610 57. Nikel PI, Romero-Campero FJ, Zeidman J a, Goñi-Moreno Á, de Lorenzo V. 2015. The Glycerol-
611 Dependent Metabolic Persistence of *Pseudomonas putida* KT2440 Reflects the Regulatory
612 Logic of the GlpR Repressor. MBio 6:1–13.
613 58. Nikel PI, Kim J, de Lorenzo V. 2014. Metabolic and regulatory rearrangements underlying
614 glycerol metabolism in *Pseudomonas putida* KT2440. Environ Microbiol 16:239–254.
615 59. Walsh M, Casey M, Kenny S, Narancic T, Blank L, Wierckx N, Ballerstedt H, O'Connor KE. 2019.
616 Insights into an alternative pathway for glycerol metabolism in a glycerol kinase deficient
617 *Pseudomonas putida* KT2440. Submitted to BioRxiv.
618 60. Tessier FJ, Monnier VM, Sayre LM, Kornfield JA. 2003. Triosidines: novel Maillard reaction
619 products and cross-links from the reaction of triose sugars with lysine and arginine residues.
620 Biochem J 369:705–719.
621 61. Benov L, Beema AF. 2003. Superoxide-dependence of the short chain sugars-induced
622 mutagenesis. Free Radic Biol Med 34:429–433.
623 62. Li XZ, Zhang L, Poole K. 1998. Role of the multidrug efflux systems of *Pseudomonas aeruginosa*
624 in organic solvent tolerance. J Bacteriol 180:2987–91.
625 63. Hishinuma S, Yuki M, Fujimura M, Fukumori F. 2006. OxyR regulated the expression of two
626 major catalases, KatA and KatB, along with peroxiredoxin, AhpC in *Pseudomonas putida.*
627 Environ Microbiol 8:2115–2124.
628 64. Sigrist CJA, de Castro E, Cerutti L, Cuche BA, Hulo N, Bridge A, Bougueleret L, Xenarios I. 2012.
629 New and continuing developments at PROSITE. Nucleic Acids Res 41:D344–D347.
630 65. Agarwal N, Kalra VK. 1983. Interaction of lanthanide cations and uranyl ion with the

631 calcium/proton antiport system in *Mycobacterium phlei*. Biochim Biophys Acta - Biomembr
632 727:285–292.
633 66. Brown PH, Rathjen AH, Graham RD, Tribe DE. 1990. Chapter 92 Rare earth elements in
634 biological systems, p. 423–452. *In* Handbook on the Physics and Chemistry of Rare Earths.
635 67. Peng L, Yi L, Zhexue L, Juncheng Z, Jiaxin D, Daiwen P, Ping S, Songsheng Q. 2004. Study on
636 biological effect of La^{3+} on *Escherichia coli* by atomic force microscopy. J Inorg Biochem 98:68–
637 72.
638 68. Mattocks JA, Ho J V., Cotruvo JA. 2019. A Selective, Protein-Based Fluorescent Sensor with
639 Picomolar Affinity for Rare Earth Elements. J Am Chem Soc jacs.8b12155.
640
641

642 # Tables

643

644 **Table 1**: Specific enzyme activities of purified PedE and PedH with the four tested growth substrates
645 at 10 mM measured with 2,6-dichlorophenolindophenol (DCPIP) dependent colorimetric assay. Data
646 represent the average of biological triplicates with according standard deviation. Activities below
647 detection limit are indicated (n. d.).

648

Substrate	Mean Specific Activity (U mg^{-1}) ± SD	
	PedE 1 mM Ca^{2+}	PedH 1 µM La^{3+}
Citrate	n.d.	n.d.
Glucose	n.d.	n.d.
Glycerol	0.3 ± 0.1	0.9 ± 0.1
2-Phenylethanol	8.0 ± 0.4	6.3 ± 0.3

649

650 **Table 2**: Lag-times (λ), maximal OD_{600} during stationary phase (OD_{600}^{max}), and maximal growth rates
651 (μ_{max}) of different *P. putida* strains during growth with M9 medium supplemented with 20 mM
652 glycerol and 0 µM or 10 µM La^{3+} incubated in microtiter plates at 30°C and 250 rpm (see also Fig. 2
653 and Fig.5). Maximal growth rates and lag-times were determined by fitting growth curves to the
654 Richards model using "grofit" package in R (44). Cultures were incubated at 250 rpm and 30°C in
655 microplate reader with constant OD_{600} measurement. Data points represent average of biological
656 triplicates with corresponding error (λ, μ_{max}) or standard deviation (OD_{600}^{max}). No growth parameters
657 could be determined for cultures that did not reach stationary phase during incubation time (n. d.).
658

Strain	λ [h]		OD_{600}^{max}		μ_{max} [h^{-1}]	
	0 µM La^{3+}	10 µM La^{3+}	0 µM La^{3+}	10 µM La^{3+}	0 µM La^{3+}	10 µM La^{3+}
KT2440*	17.3 ± 0.2	10.2 ± 0.2	0.884 ± 0.004	0.680 ± 0.014	0.341 ± 0.010	0.201 ± 0.004
Δ*pedE* Δ*pedH*	17.5 ± 0.3	17.2 ± 0.4	0.869 ± 0.002	0.802 ± 0.013	0.276 ± 0.008	0.291 ± 0.012
Δ*garK*	17.1 ± 0.3	n.d.	0.805 ± 0.005	n.d.	0.321 ± 0.011	n.d.
Δ*calA*	16.0 ± 0.3	11.1 ± 0.3	0.890 ± 0.004	0.753 ± 0.006	0.336 ± 0.011	0.271 ± 0.008
Δ*glcDEF*	17.0 ± 0.2	10.1 ± 0.2	0.862 ± 0.016	0.678 ± 0.004	0.315 ± 0.009	0.207 ± 0.004

659

660 **Table 3:** List of upregulated proteins in presence of 10 µM La^{3+} compared to the absence of La^{3+}
661 when grown with glycerol as sole C-source.
662

Locus Tag	Protein name	Fold change induction (log_2)	- log_{10}(*p*-value)
PP_2426	CalA	6.28	4.03
PP_2679	PedH	4.75	3.80
PP_3426	MexF	3.93	3.24
PP_3425	MexE	3.74	2.18
PP_4921		3.65	2.46
PP_2440	AhpF	3.13	3.08
PP_3745	GlcD	3.12	3.32
PP_3747	GlcF	2.67	3.50
PP_3746	GlcE	2.64	2.98
PP_4922	ThiC	2.21	3.84
PP_3748	GlcG	2.06	3.71
PP_3622		1.97	2.82
PP_3178	GarK	1.77	2.85
PP_3621	IorA-II	1.60	2.34
PP_0554	AcoB	1.54	2.27
PP_3623	AdhB	1.54	3.67
PP_2484		1.52	2.37
PP_0734	HemK	1.51	2.67
PP_2439	AhpC	1.39	2.02
PP_0556		1.35	2.34
PP_1125		1.30	3.01
PP_0555	AcoA	1.20	2.52
PP_1548		1.19	2.03
PP_1351	PanE	-1.45	2.06
PP_2258		-1.84	2.40
PP_5658		-1.99	2.93
PP_3557		-2.41	2.33
PP_3603		-2.46	2.73
PP_4313		-2.55	2.50
PP_0588		-2.75	2.62
PP_2674	PedE	-4.25	3.78
PP_2673		-5.37	3.71
PP_3732		-5.78	3.07

663

664 **Table S1:** Strains and plasmids used in the study

665

Strains	**Relevant features**	**Source or reference**
KT2440*	KT2440 with a markerless deletion of *upp* | Parent strain for deletion mutants	(46)
Δ*pedE*	KT2440* with a markerless deletion of *pedE*	(11)
Δ*pedH*	KT2440* with a markerless deletion of *pedH*	(11)
Δ*calA*	KT2440* with a markerless deletion of *calA*	this study
Δ*garK*	KT2440* with a markerless deletion of gene *garK*	this study
Δ*glcDEF*	KT2440* with a markerless deletion of gene cluster *glcDEF*	this study
Δ*pedE* Δ*pedH*	KT2440* with a markerless deletion of *pedE and pedH*	(11)
Δ*pedE* Δ*pedH* Δ*glpFKRD*	Δ*pedE*Δ*pedH* with a markerless deletion of gene cluster Δ*glpFKRD*	this study
E. coli TOP10	*F- mcrA Δ(mrr-hsdRMS-mcrBC) φ80lacZΔM15 ΔlacX74 nupG recA1 araD139 Δ(ara-leu)7697 galE15 galK16 rpsL(Str^R) endA1 λ$^-$*	Invitrogen
Plasmids		
pJOE6261.2	Suicide vector for gene deletions	(46)
pJOE-calA	pJOE6261.2 based deletion vector for gene *calA* (PP_2426)	this study
pJOE-garK	pJOE6261.2 based deletion vector for gene *garK* (PP_3178)	this study
pJOE-glp	pJOE6261.2 based deletion vector for gene cluster *glpFKRD* (PP_1076 to PP_1073)	this study
pMW08	pJOE6261.2 based deletion vector for gene cluster *glcDEF* (PP_3745 to PP_3747)	this study

666

667 **Table S2:** Primers used in the study

668

Primer		
Name	**Sequence 5' → 3'**	**Annealing temperature**
PcalA1	CGATGGCCGCTTTGGTCCCGAGCCGTTCCACACTTTCGC	67°C
PcalA2	AACCGATCAAGCAGGGCCTCGCAGTGAA	67°C
PcalA3	GAGGCCCTGCTTGATCGGTTGCCTGTACG	65°C
PcalA4	CCTGCAGGTCGACTCTAGAGCGTGGGTGAGCAAGGCAG	65°C
PgarK1	CGATGGCCGCTTTGGTCCCGAGTCGTTGCTGTGGTGCC	62°C
PgarK2	TACAGGGTGTGGGGTTTCTCCTGTCCTG	62°C
PgarK3	GAGAAACCCCACACCCTGTAGAAATGGCCTTATTG	67°C
PgarK4	CCTGCAGGTCGACTCTAGAGCAGCGGCAAACTGACCATC	67°C
Pglp1	CGATGGCCGCTTTGGTCCCGGTCATCAATAAAGGTCCG	55°C
Pglp2	ACCGTAGGTAGTATGACCTCGTTTTTTTTG	55°C
Pglp3	GAGGTCATACTACCTACGGTGAAGCCCTC	62°C
Pglp4	CCTGCAGGTCGACTCTAGAGGTTGTGAAGACCGCCTGC	62°C
MWH03	AGGCACGATGGCCGCTTTGGTCCCGGCCTGCTCGGGCAGTTGTTCC	63°C
MWH04	GCTAAGCATGGGCCATCGGCTCACTCGCAAC	63°C
MWH05	AGTGAGCCGATGGCCCATGCTTAGCAAGTTCGTTATCG	63°C
MWH06	GCATGCCTGCAGGTCGACTCTAGAGCCAGGGCAATGCGTATCAC	63°C

669

670 **Table S3:** List of upregulated proteins in presence of 10 µM La^{3+} compared to the absence of La^{3+}
671 when grown with 2-phenylethanol as sole C-source.
672

Locus Tag	Protein name	Fold change induction (log_2)	- log_{10}(*p*-value)
PP_2679	PedH	3.41	2.48
PP_3357	Vdh	2.65	2.92
PP_5125	MutM	2.24	3.15
PP_4905	MotA	1.84	2.01
PP_0091		1.71	2.26
PP_5157		1.59	2.20
PP_0342	WaaC	1.43	2.46
PP_3722	Alr	1.04	2.40
PP_2674	PedE	-1.49	5.90
PP_2673		-2.41	3.91

673

674 **Table S4:** List of upregulated proteins in presence of 10 µM La^{3+} compared to the absence of La^{3+}
675 when grown with glucose as sole C-source.
676

Locus Tag	Protein name	Fold change induction (log_2)	- log_{10}(*p*-value)
PP_2679	PedH	4.35	3.17
PP_4508		1.74	2.97
PP_3713	CatA	1.44	2.43
PP_5221		1.39	2.21
PP_0367		1.27	2.47
PP_4796	HolA	-1.30	2.15
PP_4374	FliT	-1.95	2.45
PP_2666		-2.01	2.51
PP_3951	PcaI	-2.13	2.68
PP_2680	AldB-II	-2.79	2.41
PP_4632	FolM	-3.54	2.53
PP_2662		-3.61	3.62
PP_1757	BolA	-3.64	3.99
PP_2674	PedE	-6.97	4.13

677

678 **Table S5:** List of upregulated proteins in presence of 10 µM La^{3+} compared to the absence of La^{3+}
679 when grown with citrate as sole C-source.
680

Locus Tag	Protein name	Fold change induction (log_2)	- log_{10}(*p*-value)
PP_2491		2.27	4.32
PP_0365	BioC	1.12	2.06
PP_4157	KdpE	-1.41	2.72
PP_2674	PedE	-2.56	2.80
PP_0634	PilA	-3.08	3.88

681

682 **Figures**

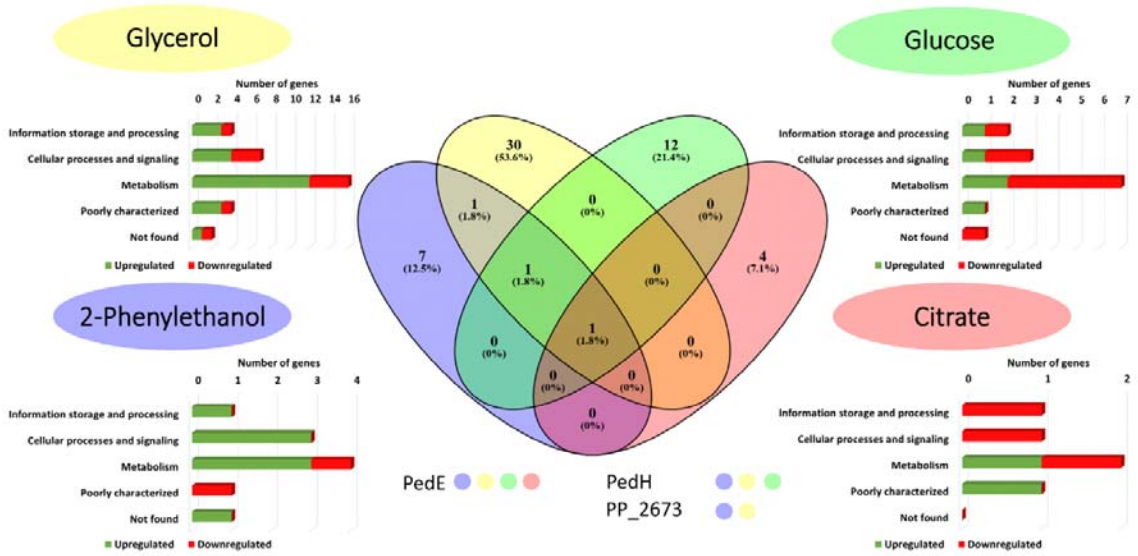

683
684
685 **Figure 1**: Venn-diagram (middle) of differentially produced proteins in response to 10 µM La^{3+} during
686 growth with glycerol, glucose, 2-phenylethanol and citrate. Proteins that showed up under several
687 growth conditions are stated under the diagram with colour code for classification (yellow dot =
688 glycerol; green dot = glucose; blue dot = 2-phenylethanol; red dot = citrate). Classifications of
689 differentially expressed proteins according to the Cluster of Orthologous Groups database are
690 depicted for each substrate.
691

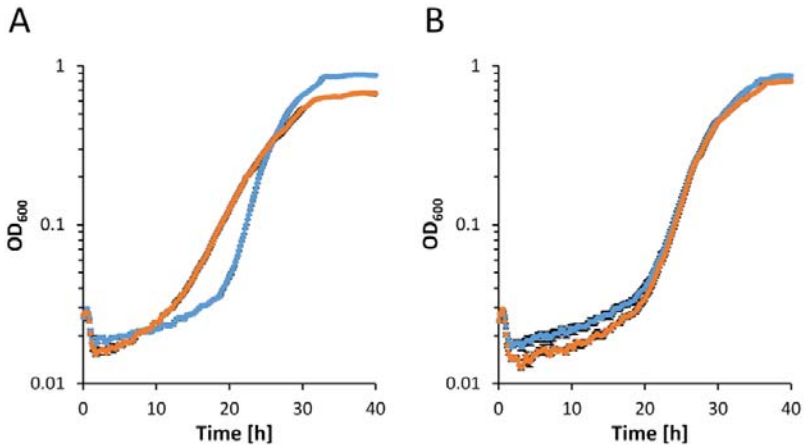

692
693
694 **Figure 2:** Growth of strains (**A**) KT2440* and (**B**) Δ*pedE* Δ*pedH* in M9 minimal medium supplemented
695 with 20 mM glycerol in the absence (blue dots) or presence of 10 µM La^{3+} (orange dots) in 96-well
696 microtiter plates at 30°C and 250 rpm. Data represent average of biological triplicates with
697 corresponding standard deviation.
698

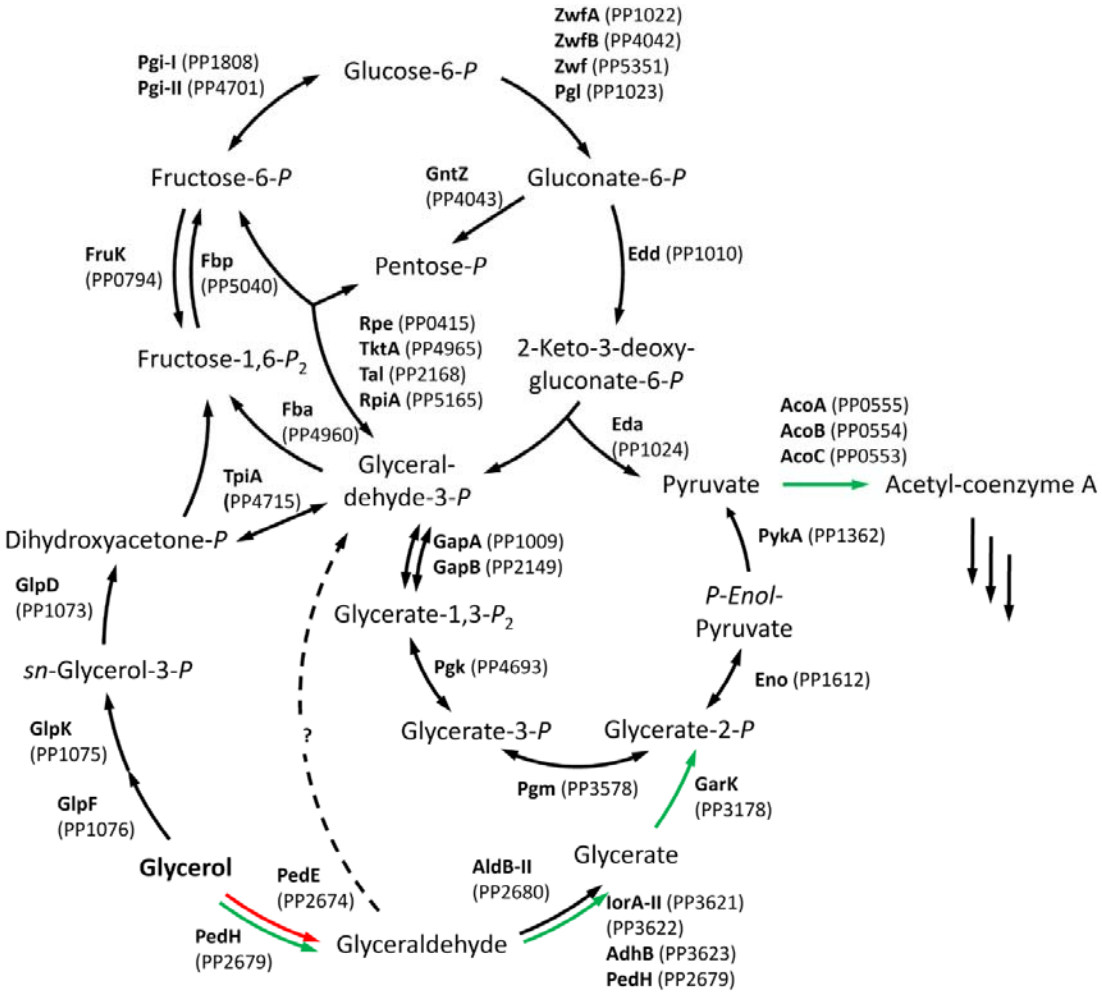

Figure 3: Proteins of the upstream central carbon metabolism of *P. putida* KT2440 including the proposed glycerol degradation pathway via glycerate and the additional hypothetical route through phosphorylation of glyceraldehyde (dotted line). Anticipated metabolic flux by the proteins that were identified as differentially abundant in response to 10 µM La^{3+} during growth on glycerol are colour-coded (green = increased, red = decreased, black = not affected). The figure is inspired by a scheme originally published by Nikel *et al.* (58) and was adapted to include the novel metabolic route(s) identified in this study.

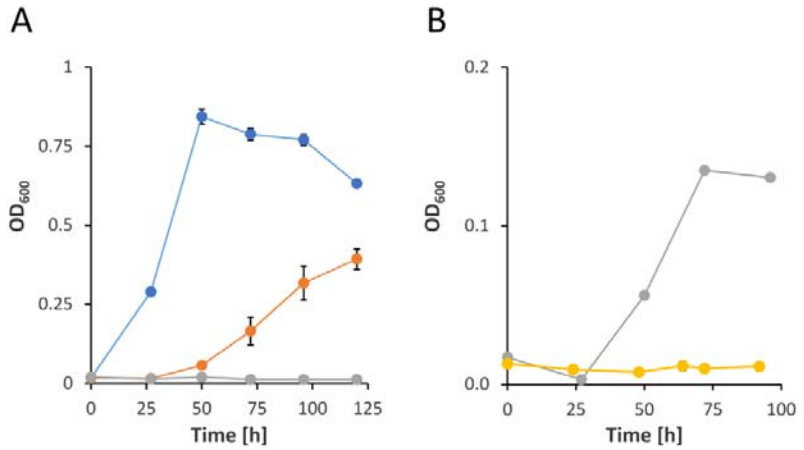

Figure 4: (**A**) Growth of strains Δ*pedE* Δ*pedH* (blue dots), Δ*glpFKRD* (orange dots), and Δ*pedE* Δ*pedH* Δ*glpFKRD* (grey dots) in M9 minimal medium supplemented with 20 mM glycerol in 96-well microtiter plates. (**B**) Growth of strains Δ*pedE* Δ*pedH* Δ*glpFKRD* (grey dots) and Δ*garK* (yellow dots), in M9 minimal medium supplemented with 20 mM DL-glycerate incubated in 96-well microtiter plates at 28°C and 220 rpm. Data represent average of biological triplicates with corresponding standard deviation.

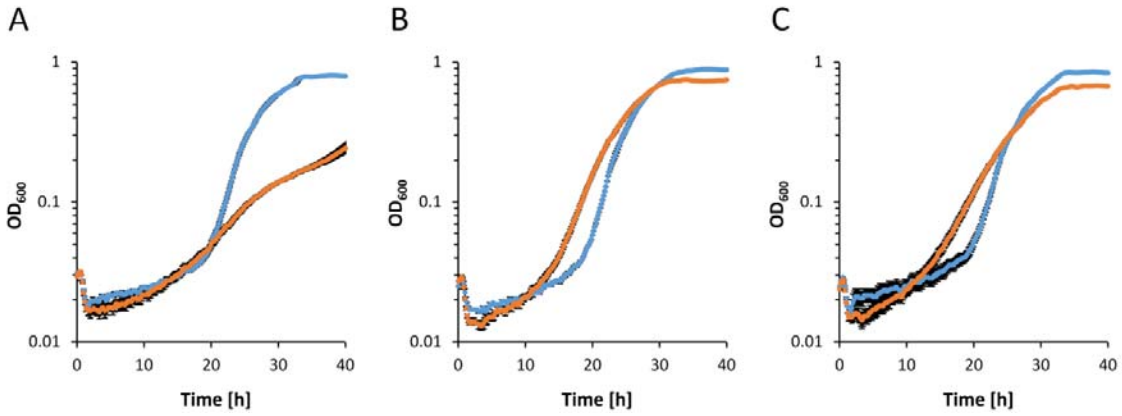

718
719
720 **Figure 5:** Growth of strains (**A**) Δ*garK,* (**B**) Δ*calA*, and (**C**) Δ*glcDEF* in M9 minimal medium
721 supplemented with 20 mM glycerol in absence (blue dots) or presence 10 µM La^{3+} (orange dots)
722 incubated in 96-well microtiter plates at 30°C and 250 rpm. Data represent average of biological
723 triplicates with corresponding standard deviation.
724

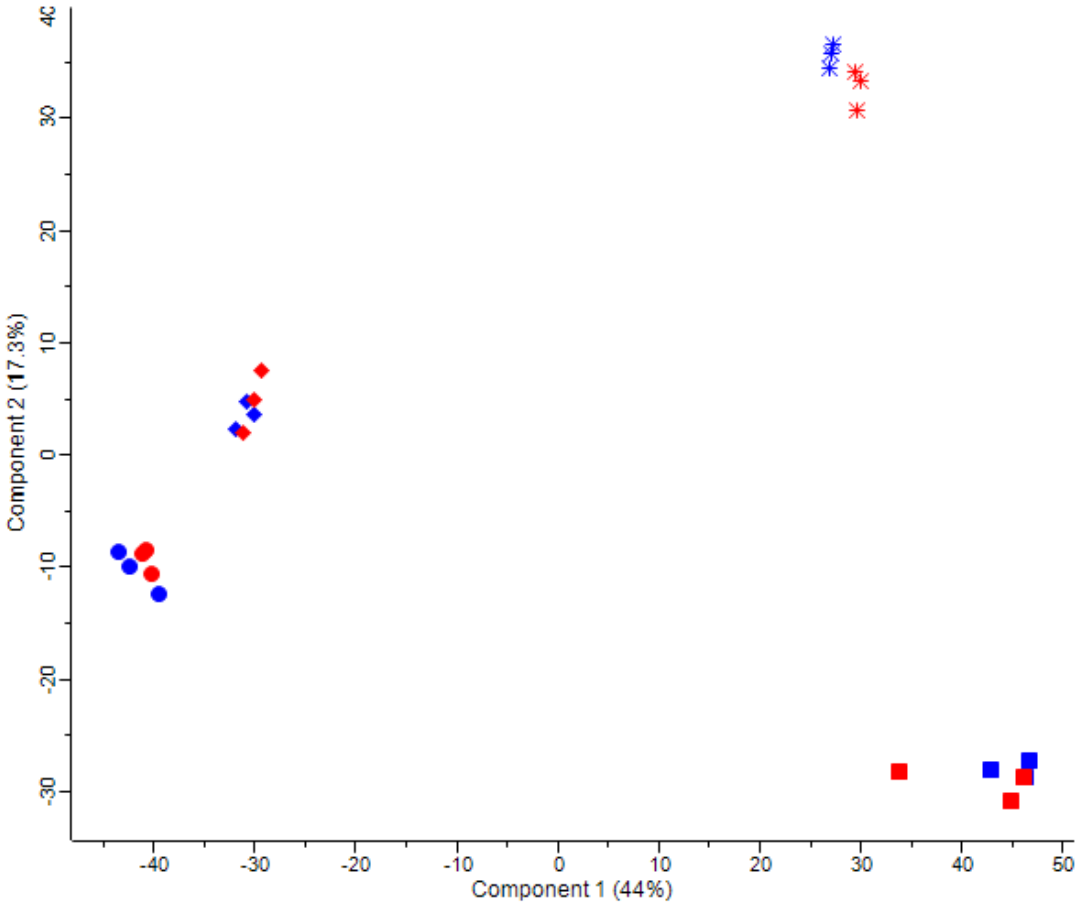

Figure S1: **PCA comparing the four different carbon sources with and without La^{3+}.** Different carbon sources are indicated by squares (2-phenylethanol), circles (citrate), diamonds (glucose) and stars (glycerol). Samples with 10 µM La^{3+} or without La^{3+} in the medium are shown in blue and red, respectively. Biological replicates are indicated in the same colour. Samples can be separated according to different carbon sources while treatment with La^{3+} only showed minor effects.